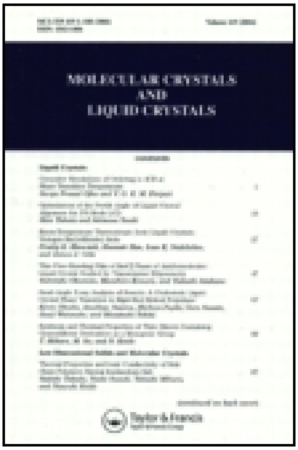

Molecular Crystals and Liquid Crystals
Publication details, including instructions for authors and subscription information:
http://www.tandfonline.com/loi/gmcl20

Raman Imaging of Nematic and Smectic Liquid Crystals

Ebru A. Büyüktanir [a], Ke Zhang [a], Arne Gericke [b] & John L. West [a]

[a] Liquid Crystal Institute, Kent State University, Kent, Ohio, USA

[b] Department of Chemistry, Kent State University, Kent, Ohio, USA

Version of record first published: 31 Aug 2012.

To cite this article: Ebru A. Büyüktanir, Ke Zhang, Arne Gericke & John L. West (2008): Raman Imaging of Nematic and Smectic Liquid Crystals, Molecular Crystals and Liquid Crystals, 487:1, 39-51

To link to this article: http://dx.doi.org/10.1080/15421400802198540

Mol. Cryst. Liq. Cryst., Vol. 487, pp. 39–51, 2008

ISSN: 1542-1406 print/1563-5287 online
DOI: 10.1080/15421400802198540

Raman Imaging of Nematic and Smectic Liquid Crystals

Ebru A. Büyüktanir[1], Ke Zhang[1], Arne Gericke[2], and John L. West[1]
[1]Liquid Crystal Institute, Kent State University, Kent, Ohio, USA
[2]Department of Chemistry, Kent State University, Kent, Ohio, USA

In this article, we demonstrate that confocal Raman microscopy can be utilized to image the director fields of liquid crystal molecules, revealing the spatial patterns of the molecular orientational order both in lateral and axial directions. Here we report on the polarized confocal Raman imaging of the electric field-aligned uniaxial nematic liquid crystal and the in-depth director profiling of the focal conic domains of smectic A liquid crystal. The C≡N stretching vibrational band [ν(CN) = 2228 cm^{-1}] and the C–C stretch of aromatic rings [ν(CC) = 1606 cm^{-1}] are used to probe the spatial director orientations of 4-pentyl-4′-cyanobiphenyl (5CB) and 4-octyl-4′-cyanobiphenyl (8CB).

Keywords: confocal Raman microscopy; cyanobiphenyl liquid crystals; focal conic domains; orientational order; smectic A

INTRODUCTION

Liquid crystals (LCs) are soft-matter systems in which molecules possess long-range orientational order [1,2] and form a variety of intricate three-dimensional (3D) molecular arrangements, such as focal conic domains in the smectic A (SmA) mesophase. Since the orientation of LCs can be changed by electric or magnetic fields, LCs have been extensively utilized in display applications. Therefore, the analysis of local LC orientation with micron resolution is of prime importance in understanding the structure of LC phases for the optimization of electro-optical devices. In order to visualize the complex spatial orientations of LC systems, non-destructive and non-invasive imaging techniques are necessary. The molecular orientational order of LCs has been studied by a number of techniques. More recent

Address correspondence to Ebru A. Büyüktanir, Liquid Crystal Institute, Kent State University, Kent, OH 44242, USA. E-mail: buyuktan@lci.kent.edu

experiments, such as fluorescence confocal polarizing microscopy [3], scanning probe microscopy [4], nuclear magnetic resonance (NMR) [5], x-ray diffraction [6], and Fourier transform infrared (FTIR) imaging spectroscopy [7], have enhanced imaging capabilities and furthered our understanding of LC structures and morphology. However, these techniques are not capable of characterizing chemical composition and orientational order for different sample depths.

Compared to other imaging techniques, non-invasive and non-destructive confocal Raman microscopy (CRM) provides a powerful way of studying the LC director field **n** both in the horizontal plane (XY-plane) and along the vertical direction (Z-axis) at a microscopic level. CRM is a vibrational spectroscopic technique that probes vibrational modes associated with specific chemical groups, and therefore presents a detailed insight into the chemical composition of the sample without requiring any molecular additives. In addition, quantitative imaging of Raman intensities can reveal information about the spatial organization of the molecules and its local environment with comprehensive 3D analysis [8].

As a micro-spectroscopic imaging technique, focal plane array FTIR (FPA-FTIR) microscopy also does not need any molecular additives and offers very high chemical selectivity. The advantage of FPA-FTIR over CRM is that it is possible to obtain a $250 \times 250\,\mu m$ image in "one shot," which means that no mapping is necessary. Conversely, the spatial resolution of FTIR microscopy is wavelength limited, resulting in lower spatial resolution ($\sim$4–12 μm) than that of CRM ($< 1\,\mu m$). More importantly, FPA-FTIR does not provide in-depth characterization, as does CRM. In this article, we demonstrate the polarized CRM imaging of the LC director fields by mapping the characteristic vibrational bands of cyanobiphenyl LCs in the horizontal plane and along the vertical direction.

EXPERIMENTAL

The Raman measurements were carried out using a Jobin Yvon HR 800 Raman Spectrometer attached to a Olympus IX71 inverted microscope. This instrument is equipped with a notch filter to prevent Rayleigh scattered light from reaching the detector. The backscattered Raman light (180°) is dispersed by a holographic transmission grating (spectral resolution $\sim 4\,cm^{-1}$) and detected by a liquid nitrogen cooled charge-coupled device (CCD) detector (1024×256 pixels). Resolution in the Z-direction of the Raman scattering was obtained by setting the confocal pinhole to 100 μm and by focusing the laser beam with a 40X microscope objective (Olympus UPlan FL, numerical aperture 0.5). The Raman signal was integrated over 2 seconds.

The spectra of LC samples were recorded using 632.8 nm He-Ne laser in the spectral range 0 to 3000 cm^{-1} at room temperature. The power of the laser was decreased from 20 mW to 5 mW at the source by using a neutral filter to prevent possible local temperature increase due to strong light absorption. The Raman spectrometer wavelength range was calibrated prior to the experiment by using the silicon phonon line at 520 cm^{-1}. The He-Ne laser beam was modified by means of a linear polarizer **P**, which was placed parallel to the partially polarized excitation beam.

All the Raman images were obtained through mapping, a technique based on point-by-point scanning of the selected area of the sample using the motorized X-Y microscope stage (stepwidth 1.4 μm). The color-coded images (i.e., plots of spectral parameter versus the X-Y

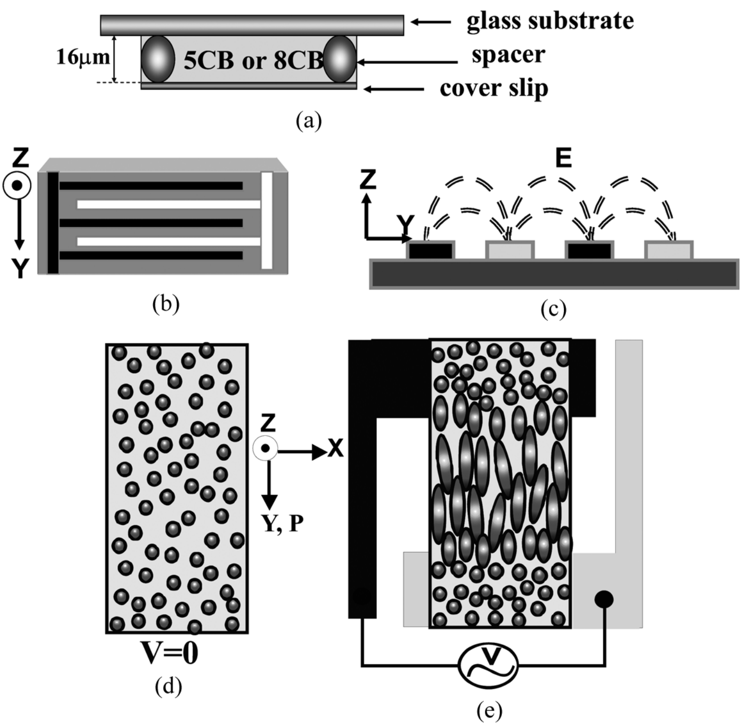

FIGURE 1 (a) The LC cell configuration used to perform Raman experiments. (b) The illustration of the top view of the interdigitated ITO electrodes and (c) the side view of the applied E-field direction between interdigitated ITO electrodes. (d) The LC director field in an interdigitated nematic LC cell with homeotropic alignment at a zero applied E-field (e) and at an applied **E**-field. **P** stands for the polarization direction of the laser beam.

coordinates of the respective sampling point) were produced with LabSpec 4.02 (HORIBA Jobin Yvon, Inc.) and further analyzed with Isys40 Chemical Imaging Software (MathWorks, Inc.), providing the spatial intensity distribution of the ν(CN) or ν(CC) Raman bands of a chosen area on the LC sample.

To perform the Raman experiments, we prepared typical LC cells as shown in Fig. 1(a). An indium-tin-oxide (ITO) coated glass substrate (Corning, 1.1 mm thick) and a cover slip (Fisher Scientific, 0.1 mm thick) were used as cell substrates. The cell thickness d was controlled by using 16 μm spacers. The interdigitated electrodes on the ITO-coated glass substrate (Fig. 1(b)) were etched by standard photolithography. For homeotropic alignment of the LC director, both of the substrates were spin-coated with PI7511 (Nissan). Next, 5CB (EMD Chemicals, Inc.) was capillary-filled into the preassembled empty cell at 60°C. Afterwards, in-plane switching of the LC molecules in the cell was achieved by applying an AC electric field (**E**-field) of 1 kHz. The **E**-field lines in between the two interdigitated electrodes are sketched in Fig. 1(c). The electric fields point in opposite directions near the edges of the electrodes. This type of cell design has been used as an in-plane switching mode for LC displays. To minimize the spherical aberrations during imaging, the cover slip side of the cell was placed above the microscope objective. 8CB (Aldrich) and 5CB were used without further purification.

RESULTS AND DISCUSSION

The Raman Mapping of Field-Aligned Nematic Liquid Crystals

Here we studied the electric field-induced orientation of 5CB molecules. Uniaxial cyanobiphenyl LCs (Fig. 2) are very strong Raman scatterers; therefore, a good signal-to-noise spectrum can easily be obtained. The average orientation of cyanobiphenyl LC molecules can be determined by probing the Raman active C=C double and C≡N triple bond vibrational modes with a linearly polarized laser beam. If the electric field vector of an incident plane polarized light **P** lies along the long axis of cyanobiphenyl compounds, a higher Raman intensity is obtained [9].

Initially, the LC director "**n**" is parallel to the Z-axis ($n_x = 0$, $n_y = 0$, $n_z = 1$), which is due to the homeotropic boundary condition (Fig. 1(d)). The reorientation of LCs in the presence of an external field is known as Freedericksz transition [10]. If LC molecules posses a positive dielectric anisotropy ($\Delta\varepsilon > 0$), the director **n** tends to align parallel to the applied field. Since 5CB molecules possess a positive $\Delta\varepsilon$, the

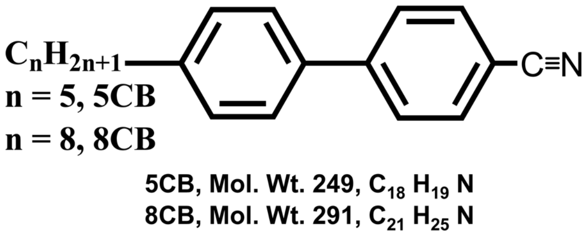

FIGURE 2 The chemical structure of 5CB (4-pentyl-4′-cyanobiphenyl) LC and 8CB (4-octyl-4′-cyanobiphenyl) LC.

applied AC electric (**E**) field above the Freedericksz threshold [10] distorts the director field. The reoriented director field along the **E**-field lines between the two interdigitated electrodes is shown in Fig. 1(e). Later, we recorded the Raman scattering signals from the planar ($\mathbf{n}\|$Y-axis) and homeotropic ($\mathbf{n}\|$Z-axis) regions of the interdigitated 5CB cell in the spectral range from 0 to 3000 cm^{-1} during the application of the **E**-field. During this measurement, the polarization direction of the incident laser light **P** was set along the Y-axis. Typical Raman spectra for planar and homeotropic orientations of 5CB LC are shown in Fig. 3(a). The different band intensities were observed because 5CB molecules possess an anisotropic Raman tensor giving rise to Raman intensity variations for different orientations. This difference is more pronounced for the C=C band in the aromatic ring and the C≡N group, which are both located along the long axis of the molecule. Besides the C≡N stretch (2228 cm^{-1}) and the C−C stretch of the aromatic ring (1606 cm^{-1}) vibrational bands, the C−C stretch of the biphenyl link (1286 cm^{-1}) and C−H in-plane deformation (1180 cm^{-1}) vibrational bands of 5CB molecules can also be used for orientational order analysis (Fig. 3). However, in order to achieve Raman images with high resolution and contrast, we selected either ν(CC) or ν(C≡N) bands.

The next step in this study was to use this model system to show the capabilities of CRM mapping. In order to visualize the molecular orientations of the field-aligned 5CB cell, we recorded the C≡N stretching vibrational band in the range of 2200–2250 cm^{-1} (Fig. 3(b)). The optical microscopy and the two-dimensional (2D) Raman image (integrated C≡N stretching band intensity) of the X-Y mapped area are depicted in Figs. 4(a) and (b), respectively. From this Raman image, we can easily extract and confirm the field-oriented LC spatial profile shown in Fig. 1(e) on the XY-plane. In this configuration, the LC molecules align homeotropically in the field-off state ($\mathbf{E} = 0$ V), while in the field-on

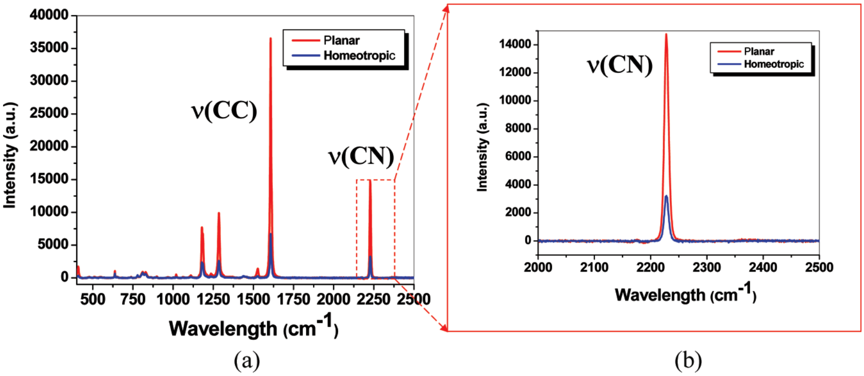

FIGURE 3 (a) Raman spectra of a field-aligned 5CB cell and (b) the C≡N stretching vibrational band spectrum at planar and homeotropic regions of the cell. Measurements were performed at room temperature.

state the fringing field pattern occurs and the LC director distortion develops in between the interdigitated electrodes. The electric fields point in opposite directions near the edges of the electrodes. The maximum intensity of the Raman C≡N stretching band intensity is located in the regions where $\mathbf{n}\|\mathbf{P}$, and the minimum intensity is located

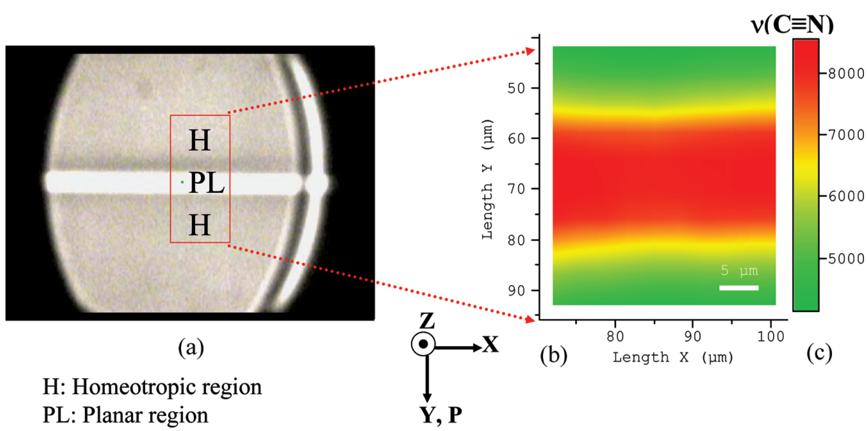

FIGURE 4 (a) Optical microscopy image and (b) 2D Raman image of the interdigitated 5CB LC cell upon application of the **E**-field. (c) The color bar represents the relative Raman intensity of the ν(C≡N) stretching band of the mapped area. The polarization direction of the laser beam, or **P**, is along the Y-axis.

in the regions where $\mathbf{n} \perp \mathbf{P}$. LC molecules in the middle of the electrodes stay parallel to the cell normal ($\mathbf{n} \| z$ and $\mathbf{n} \perp \mathbf{P}$), giving rise to a low Raman intensity region, as seen in Fig. 4(b). The color scale on the Raman images shows the change in the orientation of the $\nu(C{\equiv}N)$ stretching band (Fig. 4(c)) in the mapped area. As a result, we concluded that polarized confocal Raman microscopy is very sensitive to the orientation of the LC molecule and can be utilized to study the LC director orientation explicitly.

The Raman mapping of focal conic domains

Smectic A liquid crystals are one-dimensional (1D) periodic condensed matter structures. Like nematic LCs, smectics exhibit long-range orientational order. SmA LCs form layered structures with 1D translational order where the centers of mass of the molecules are arranged in a direction normal to the layers. They exhibit 1D quasi-long range order rather than true long-range positional order, as in crystals. This phase is considered a 2D liquid, which possesses the freedom of molecular motion within the layer, but is hindered from translation from one layer to the next [1].

SmA layers usually form topological defects to satisfy the boundary conditions at a low cost of energy. The most common type of structural defects in layered or lamellar LC phases are so-called *focal conic domains* (FCDs), which were first observed by G. Friedel and F. Grandjean [11]. The vertical cross-section of a typical FCD is schematically depicted in Fig. 5, which shows an FCD of the first species, or FCD-I. In FCD-I, the smectic layers bend in such a way that layers preserve the thickness while adopting the shape of Dupin cyclides, i.e., surfaces whose lines of curvature are circles. A family of Dupin cyclides consists of singular lines as a pair of one branch of a hyperbola **H** and an ellipse **E** located in two orthogonal planes where the apices of any of **H** and **E** are at the foci of the other [2,11–16].

The formation of FCDs can be induced when the SmA material is contained in a bound volume or exposed to the external fields. In both cases, the constant layer thickness is preserved as a result of the layers relaxing during the formation of the one-dimensional FCD structure. Additionally, the thickness of smectic layers is very sensitive to temperature changes. Thus, static layer distortions—such as layer undulations and FCDs—can occur as the result of significant temperature variations or bulk/surface irregularities in the cell [17]. In order to visualize FCDs by CRM, we prepared 8CB LC cells without using any alignment layer on the glass substrate and the cover slip. The cell was filled at 60°C (well above the isotropic phase transition

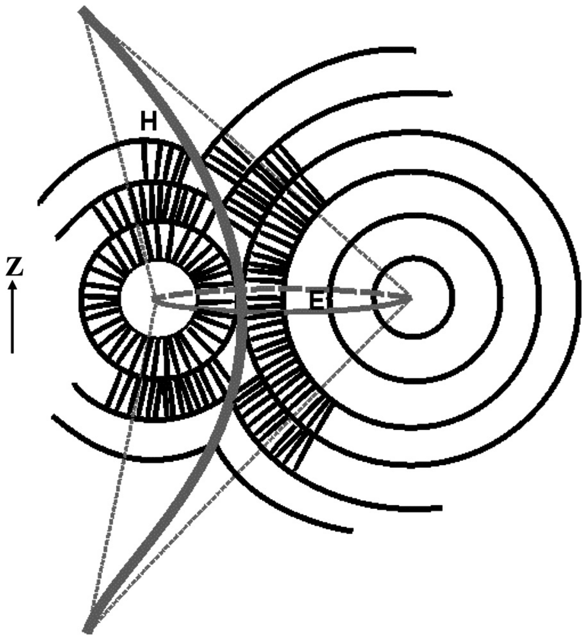

FIGURE 5 The schematic representation of the vertical cross-section of FCD of the first species (FCD-I) along the Z-axis. The SmA layers curve around the confocal ellipse (**E**) and the hyperbola (**H**).

temperature $T_{NI} = 40.5°C$) and subsequently fast-cooled to room temperature, at which the 8CB is in the SmA phase ($T_{NA} = 33.5°C$). Finally, the cell was sealed with epoxy glue.

After assembling a 16 μm thick 8CB cell, the FCD-I was first imaged by using optical microscopy with crossed polarizers as presented in Fig. 6(a). Later, the X-Y coordinates on the visible image of the sample (Fig. 6(b)) were selected for Raman imaging. Figure 6(c) shows the polarized CRM image of the FCD-I defect, where **P** was along the Y-axis. As shown in the 2D Raman image (obtained by integrating the intensity of the C≡N stretching vibration band) of the FCD-I defect, the maximum Raman intensity was registered in the regions where the LC director was parallel to the polarization direction of a laser beam (**P**||**n**). As **n** deviates from **P**, the intensity decreases. The director field **n** of the horizontal cross-section of FCD-I is shown in Fig. 6(d). The dashed lines represent the director field **n**.

In the second set of experiments, the polarization direction of the light **P** was set along the X-axis (Fig. 7(a)). This was achieved by

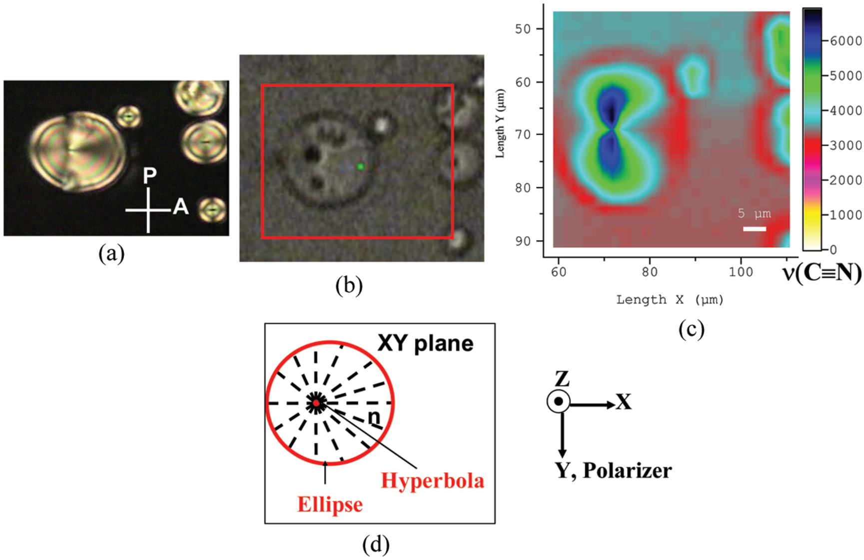

FIGURE 6 (a) The optical microscopy image of FCD-I with crossed polarizer (P) and analyzer (A); (b) the visible image of the defect; (c) 2D Raman image of (b) when polarizer **P** is set along the Y-axis. (d) The director field n of the horizontal cross-section of FCD-I is reconstructed from the 2D Raman image. The dashed lines represent the director field **n**.

rotating the LC sample by 90°. Figure 7(b) shows the mapped 2D Raman image (the aromatic ν(CC) stretching band intensity) of the FCD-I as the **P**‖X-axis. The eccentricity and the size of the FCD-I in Fig. 7 were very similar to those of the FCD-I seen in Fig. 6. Note that the combination of Fig. 7 (**P**‖X-axis) and Fig. 6 (**P**‖Y-axis) completes the director fields of the FCD-I defect structure on the horizontal plane (Fig. 6(d)). In order to prove the in-depth capability of the CRM, we visualized the FCD-I along the Z-axis. Therefore, the microscope objective was focused at different depths of the cell by moving the focal plane down the Z-direction. The Raman spectra of this FCD-I (see visible image in Fig. 7(a)) were collected with a 1.4 µm step size in X and Y directions and a 5 µm step size along the Z-axis, which was labeled as Z1 to Z16 on the graphs. Since the signal-to-noise ratio and the Raman intensity ratio of planar to homeotropic alignment for the aromatic ν(CC) stretching vibrations are larger than those of the ν(C≡N) (see Fig. 3), in this configuration (**P** ‖ X-axis) both the 2D Raman mapping and in-depth profiling of FCD-I were carried out by using the ν(CC) symmetrical stretching mode of the benzene rings in the

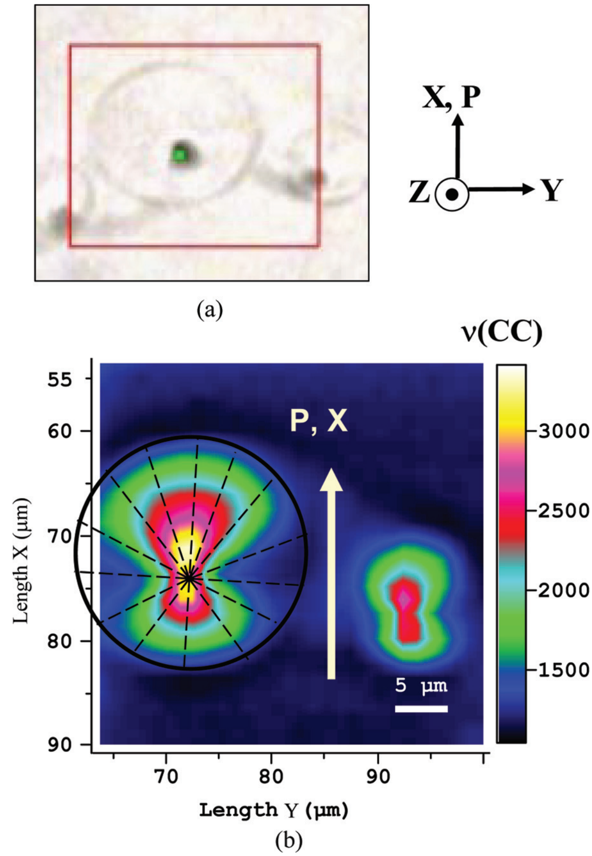

FIGURE 7 (a) The optical microscopy and (b) 2D Raman image of the FCD-I on the XY plane, where the **P** was set along the X-axis. The director field (dashed lines) is drawn on the Raman image. The color bar in (b) represents the relative Raman intensity of the ν(CC) stretching band of the mapped area. The diameter of the FCD-I is $\sim$20 μm.

biphenyl group at 1606 cm^{-1}. The collected Raman spectra from each of the X-Y segments between Z1 and Z16 were reprocessed by Isys40 Imaging Software. This allowed us to plot all 2D Raman images in 3D graphical representation in the same color scale as shown in Fig. 8(a), where the vertical axis on the plots represents the collected Raman intensity at each point. Once we analyzed all these data, which contain molecular orientational information of FCD-I, we were able to rebuild the director fields in the vertical direction. Figure 8(b) illustrates the reconstructed director field of FCD-I along the Z-axis.

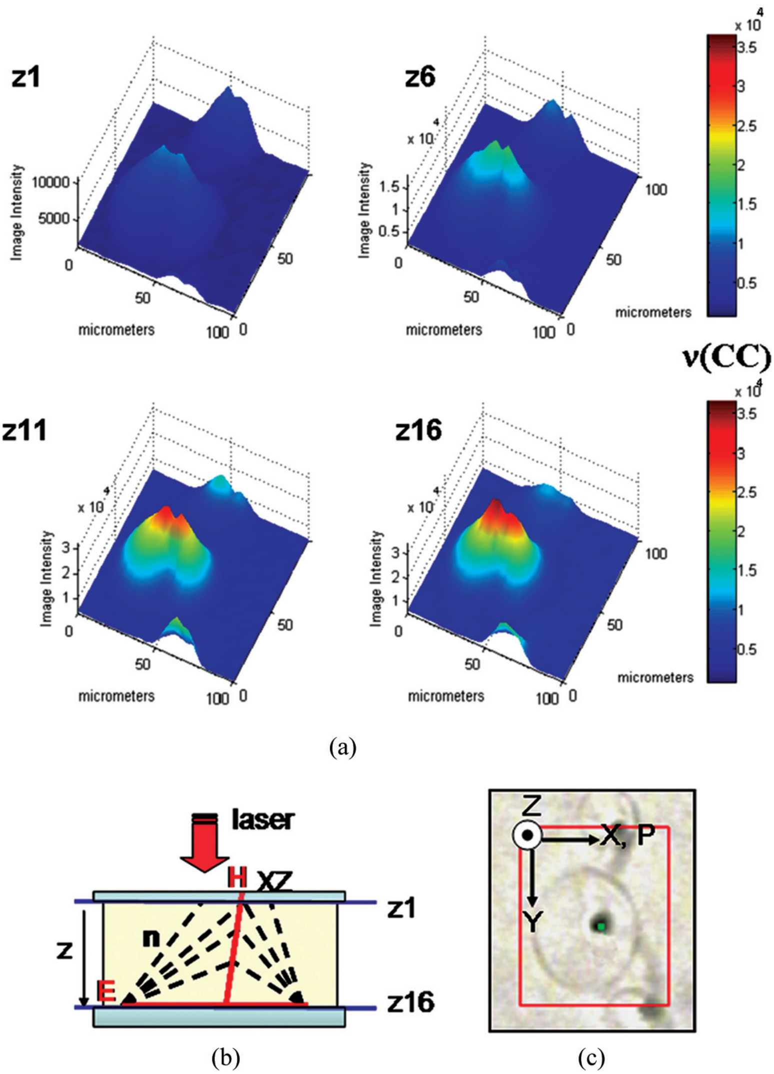

FIGURE 8 (a) The Raman images of the FCD-I in 3D graphical representations at different depths (along the Z-axis) of the cell, where z1 is closer to the cover slip side of the cell. (b) The illustration of the corresponding director field **n** constructed along the vertical (XZ) plane, which contains half of the hyperbola **H** and the ellipse **E**. (c) The optical microscopy image of the defect. The base of the defect is located on the surface of the cell. The color bar in (a) represents the relative Raman intensity of the ν(CC) stretching band of the mapped area.

Here we can clearly observe the ellipse, the tip of the hyperbola and the director pattern change from Z1 to Z16. The Raman images of FCD-I indicate that the ellipse is located on the bottom substrate. These results are in very good agreement with theoretical studies and computer simulations of FCDs reported earlier in the literature [12–16].

In this study, the main factor that limits the Z-resolution is the birefringence of the liquid crystal materials. This birefringence-induced defocusing gives rise to distorted images of the selected volume. This aspect of a confocal imaging system has been discussed in detail in reference [18]. According to this reference, the spatial defocusing of the anisotropic media is estimated roughly as $g\Delta nz/n_{ave}$, where g is a geometrical term ($g = 1$), Δn is the birefringence, z is the depth of the scanning, and n_{ave} is the average refractive index of the medium. Even though 5CB and 8CB are relatively high birefringent LCs, we kept the cell thickness very thin to reduce the defocusing effect to a minimum. For example, the axial resolution (in-depth resolution) at the LC cell thickness of $z \sim 10\,\mu m$ is only $\sim 1\,\mu m$ for 8CB ($\Delta n \sim 0.16$, and $n_{ave} \sim 1.6$).

CONCLUSION

We have successfully demonstrated that CRM imaging can be utilized to study the molecular orientation of LC molecules. We showed that Raman chemical imaging of different layers of smectic LC materials in the interior of a sample provides a “fingerprint” of the sample’s molecular orientation and composition. Our results demonstrated that confocal Raman microscopy is a remarkable, simple, and very sensitive optical technique to study LC director fields in confined geometries. This method can be applied to not only thermotropic liquid crystals, but also lyotropic liquid crystals. Finally, CRM imaging technology opens up new possibilities in material research because depth profiling gives researchers the capability to work in the third dimension.

REFERENCES

[1] De Gennes, P. G. & Prost, J. (1998). *The Physics of Liquid Crystals*, (2nd Edition), Oxford Science Publications, Clarendon Press: Oxford, Chapter 1.
[2] Kleman, M. & Lavrentovich, O. D. (2003). *Soft Matter Physics: An Introduction*, Springer Verlag: New York, p. 668.
[3] Smalyukh, I. I., Shiyanovskii, S. V., & Lavrentovich, O. D. (2001). *Chem. Phys. Lett.*, *336*, 88–96.

[4] Walba, D., Stevens, F., Parks, D., Clark, N. A., & Wand, M. D. (1995). *Science*, *267*, 1144.
[5] Sandström, D., Komolkin, A. V., & Maliniak, A. (1996). *J. Chem. Phys.*, *104*(23), 9620.
[6] Acharya, B. R., Primak, A., & Kumar, S. (2004). *Phys. Rev. Lett.*, *92*, 145506.
[7] McFarland, C. A., Koening, J. L., & West, J. L. (1993). *Appl. Spectrosc.*, *47*(3), 321.
[8] Pastorczak, M., Wiatrowski, M., Kozanecki, M., Lodzinski, M., & Ulanski, J. (2005). *J. of Mol. Struct.*, *744*, 997.
[9] Jones, W. J., Thomas, D. K., Thomas, D. W., & Williams, G. (2004). *J. of Mol. Struct.*, *708*, 145–163.
[10] Blinov, L. M. & Chigrinov, V. G. (1994). *Electrooptic Effects in Liquid Crystal Materials*. Springer-Verlag: New York.
[11] Friedel, G. (1922). *Annales de Physique*, *18*, 273–474 and Grandjean, F. (1916). *Bull. Soc. Fr. Mineral*, *39*, 164 in Sluckin, T., Dunmur, D., & Stegemeyer, H. (2004). *Crystals that Flow*, Taylor & Francis: New York, 163 and 128.
[12] Kleman, M. (1977). *Le Journal De Physique*, *38*, 1511.
[13] Fournier, J. B. & Durand, G. (1991). *J. Phys. II France*, *1*, 845–870.
[14] Boltenhagen, P., Lavrentovich, O. D., & Kleman, M. (1992). *Phys. Rev. A*, *46*(4), R1743.
[15] Kleman, M. (1992). *Phys. Rev. A*, *46*, R1743.
[16] Kleman, M. & Lavrentovich, O. D. (2000). *Phys. Rev. E*, *61*(2), 1574.
[17] Krentsel, T. A., Lavrentovich, O. D., & Kumar, S. (1997). *Mol. Cryst. Liq. Cryst.*, **304**, 463–469.
[18] Shiyanovskii, S. V., Smalyukh, I. I., & Lavrentovich, O. D. (2001). Computer Simulations and Fluorescence Confocal Polarizing microscopy of Structures in cholesteric Liquid Crystals (Chapter 10). In: *Defects in Liquid Crystals: Computer Simulations, Theory and Experiment*, Lavrentovich, O. D., Pasini, P., Zannoni, C., et al. (Eds.), Kluwer Academic Publishers: The Netherlands, 229–270.